CrossMark

HEAD AND NECK

Comparison of intravoxel incoherent motion diffusion-weighted imaging between turbo spin-echo and echo-planar imaging of the head and neck

Ryoji Mikayama[1] · Hidetake Yabuuchi[1] · Shinjiro Sonoda[2] · Koji Kobayashi[2] ·
Kazuya Nagatomo[1] · Mitsuhiro Kimura[1] · Satoshi Kawanami[3] · Takeshi Kamitani[3] ·
Seiji Kumazawa[1] · Hiroshi Honda[3]

Abstract

Objectives To compare image quality, apparent diffusion coefficient (ADC), and intravoxel incoherent motion (IVIM)-derived parameters between turbo spin-echo (TSE)-diffusion-weighted imaging (DWI) and echo-planar imaging (EPI)-DWI of the head and neck.

Methods Fourteen volunteers underwent head and neck imaging using TSE-DWI and EPI-DWI. Distortion ratio (DR), signal-to-noise ratio (SNR), contrast-to-noise ratio (CNR), ADC and IVIM-derived parameters were compared between the two techniques. Bland-Altman analysis was performed to analyse reproducibility between the quantitative parameters of TSE-DWI and EPI-DWI.

Results DR of TSE-DWI was significantly smaller than that of EPI-DWI. SNR and CNR of TSE-DWI were significantly higher than those of EPI-DWI. ADC and IVIM-derived parameters of TSE-DWI showed higher values than those of EPI-DWI, although the difference was not significant. Bland-Altman analysis showed wide limits of agreement between the two sequences.

Conclusion TSE-DWI can produce better image quality than EPI-DWI, while TSE-DWI possibly exhibits different values of quantitative parameters. Therefore, TSE-DWI could be a good alternative to EPI-DWI for patients sensitive to distortion. However, it is not recommended to use both TSE-DWI and EPI-DWI on follow-up.

Key points
• *Head and neck DWI is especially sensitive to magnetic inhomogeneity.*
• *The distortion of images was less with TSE-DWI than with EPI-DWI.*
• *TSE-DWI can possibly exhibit higher ADC and IVIM-derived parameters than EPI-DWI.*
• *Bland-Altman analysis showed unacceptable LoA in quantitative analysis between TSE-DWI and EPI-DWI.*
• *It is not recommended to use both TSE-DWI and EPI-DWI for follow-up.*

Abbreviations

ADC	Apparent diffusion coefficient
D	Pure diffusion coefficient
DR	Distortion ratio
DWI	Diffusion-weighted imaging
EPI	Echo-planar imaging
f	Perfusion fraction
IVIM	Intravoxel incoherent motion
SENSE	Sensitivity encoding
TSE	Turbo spin-echo

✉ Hidetake Yabuuchi
  h-yabu@med.kyushu-u.ac.jp

1 Department of Health Sciences, Graduate School of Medical Sciences, Kyushu University, 3-1-1 Maidashi, Higasi-ku, Fukuoka 812-8582, Japan

2 Division of Radiology, Department of Medical Technology, Kyushu University Hospital, 3-1-1 Maidashi, Higasi-ku, Fukuoka 812-8582, Japan

3 Department of Clinical Radiology, Graduate School of Medical Sciences, Kyushu University, 3-1-1 Maidashi, Higasi-ku, Fukuoka 812-8582, Japan

Introduction

Diffusion-weighted imaging (DWI), which assesses the degree of diffusion of water molecules in living tissues, has become one of the most essential techniques for the detection of various diseases, such as acute cerebral infarction, neoplasm and inflammatory lesions [1–4]. The apparent diffusion coefficient (ADC) reflects the quantitative diffusivity of protons; this might be useful in the differentiation of diseases and prediction of treatment response and prognosis [5, 6]. However, ADC cannot separate the perfusion that represents the capillary blood flow from the diffusion of water molecules. Therefore, ADC cannot accurately determine the degree of diffusion of water molecules.

Contrarily, intravoxel incoherent motion (IVIM) imaging, which is a DWI technique, can evaluate diffusion and perfusion separately using multiple b-values [7]. IVIM imaging yields the three quantitative parameters (D, D* and f) that represent the true diffusion coefficient, pseudo-diffusion coefficient and perfusion fraction, respectively. These IVIM-derived parameters can also facilitate differential diagnosis and estimations of therapeutic effects as well as ADC [8, 9]. However, the image quality of standard single-shot echo-planar imaging (EPI)-DWI (EPI-DWI) is frequently deteriorated by susceptibility artefacts, because EPI sequence is prone to phase error accumulation. Moreover, the head and neck area is especially sensitive to magnetic inhomogeneity due to the presence of dental alloy or its complex structure with many boundaries, such as air or bones. These susceptibility artefacts cause image distortion or signal loss, and they may hamper accurate disease detection or measurements of ADC and IVIM-derived parameters [10].

The single-shot turbo spin-echo (TSE) is the second most common DWI sequence [11]. Importantly, DWI using the spin-echo based TSE sequence (TSE-DWI) is less sensitive to susceptibility artefacts, because it uses radio frequency (RF) refocusing pulses [12–14]; however, the scan time of this sequence is long due to multiple RF refocusing pulses and the RF heating restrictions with an increase in the specific absorption rate. In recent years, TSE-DWI has been improved by the adoption of the modulus averaging method, short RF pulses and sensitivity encoding (SENSE) [15]. Elefante et al. have recently reported that multi-shot TSE-DWI has higher sensitivity for detection of cholesteatoma and lower probability of misdiagnosis compared with single-shot EPI-DWI [16]. We hypothesised that TSE-DWI can improve DWI quality and can be used as an alternative sequence for EPI-DWI in the head and neck. The reproducibility of ADC values between EPI-DWI and TSE-DWI and the comparison of IVIM parameters in normal pituitary gland between EPI-DWI and TSE-DWI have already been reported [17, 18]; however, there have been no reports comparing the IVIM-derived parameters between TSE-DWI and EPI-DWI of the head and neck. Thus,

the purpose of our study was to compare the image quality, ADC and IVIM-derived parameters of TSE-DWI and EPI-DWI of the head and neck using a 3-T magnetic resonance (MR) unit.

Materials and methods

Subjects

All experiments were performed after obtaining institutional review board approval and written informed consent from all subjects. The inclusion criteria were as follows: no present illness of the head and neck areas, no contraindication for MR examinations including claustrophobia or presence of metallic biomedical materials or electronic devices in the body. We excluded patients who had metallic artificial dentition or dental bridges, because they would cause severe susceptibility artefacts in MR images. Fourteen healthy volunteers (seven men and seven women; age range, 21–23 years; mean age, 22 years) prospectively underwent DWI of the head and neck.

Imaging protocol

MR imaging was performed using a 3-T magnetic resonance system (Intera Achieva 3.0 T TX, Philips Healthcare, Best, The Netherlands) with a 16-channel SENSE Neurovascular coil. The axial TSE-T2-weighted imaging (T2WI) was performed with the following parameters: repetition time, 3,000 ms; echo time, 80 ms; field of view, 230×230 mm^2; matrix size, 336×336; slice thickness, 5 mm with a 1-mm intersection gap. The slice thickness of 5 mm was chosen for T2WI to allow superimposition using DWI. Diffusion-weighted MRI data were acquired using both single-shot TSE sequence and single-shot EPI sequence. The single-shot TSE sequence had the following parameters: repetition time, 4,200 ms; echo time, 78.8–81.3 ms; field of view, 230×230 mm^2; matrix size, 128×129; reconstruction matrix size, 320×320; reconstruction voxel size, 0.72 mm; SENSE factor, 2.0; Partial Fourier factor, 0.6; TSE factor, 40; slice thickness, 5 mm with a 1-mm intersection gap; bandwidth, 630 Hz/pixel; number of signal averages, 4; b value = 0, 300 and 750 s/mm^2; fat suppression, spectral pre-saturation with inversion recovery; acquisition time, 8 min 24 s. The parameters of the single-shot EPI sequence were as follows: repetition time, 6,000 ms; echo time, 71.5–72.7 ms; field of view, 230×230 mm^2; matrix size, 128×125; reconstruction matrix size, 320×320; reconstruction voxel size, 0.72 mm; SENSE factor, 2.5; Partial Fourier factor, no; EPI factor, 51; slice thickness, 5 mm with a 1-mm intersection gap; bandwidth in frequency direction, 2,820 Hz/pixel; number of signal averages, 4; b value = 0, 300 and 750 s/mm^2; fat suppression, short-T1

inversion recovery; acquisition time, 1 min 42 s. These two DWI sequences were consecutively performed in each examination. Fujima et al. reported that the signal intensity in the high b-value might be an outlier because the decrease was small compared to that in the low b-value, and the calculated parameters were probably influenced by this outlier [19]. For shortening the scanning time, we chose b = 0, 300 and 750 s/mm^2 [8, 9, 19].

Data analysis

Image quality

The quantitative assessments of image quality of all the volunteers were analysed by a radiological technologist under the guidance of an experienced radiologist (26 years' experience in head and neck radiology). The image distortion in the phase-encoding direction, signal-to-noise ratio (SNR) and contrast-to-noise ratio (CNR) from TSE-DWI and EPI-DWI (with b = 750 s/mm^2) were noted. For the evaluation of distortion, fusion images were created by superimposing T2WI and DWI findings using DxMM (Medasys, Gif-sur-Yvette, France) without use of an automatic position registration (Fig. 1a). Image distortions of each sequence at cervical spinal cords at the nasopharynx and oropharynx levels, submandibular glands, palatine tonsils and cerebellar hemispheres were quantitatively compared using the distortion ratio (DR). The DR is defined as per the following equation:

$$DR = A \big/ B \tag{1}$$

A is the maximum displacement in the phase-encoding direction of the anatomical structure between T2WI and each-DWI, and B is the diameter in the phase-encoding direction of the anatomical structure on TSE-T2WI (Fig. 1a) [20].

At least three circular regions of interest (ROIs) of 50 pixels were set in the submandibular glands and parotid glands in order to measure the SNR and CNR. However, superior deep cervical lymph nodes in normal volunteers were too small to set three ROIs; therefore, we used a single ROI, as large as possible, within a superior deep cervical lymph node. For the reference tissue of CNR measurements, 50 pixel ROIs were set at muscles close to each organ. The SNR and CNR were calculated from each ROI, defined by the following equations:

$$SNR = SI_a \big/ SD_a \tag{2}$$

$$CNR = \left| SI_a - SI_{muscle} \right| \big/ SD_{muscle} \tag{3}$$

where SI_a is the mean signal intensity in the anatomical regions, SD_a is the standard deviation of signal intensity in the anatomical regions, SI_{muscle} is the mean signal intensity in the muscle and SD_{muscle} is the standard deviation of the

signal intensity in the muscle. The mean SNR and CNR of multiple ROIs were calculated at the submandibular glands and parotid glands. Noise measurement with parallel imaging was difficult because the noise level in the reconstructed images largely depends on the sensitivity profiles of receiver coils; noise distribution is heterogeneous for each given location [21]. Therefore, we used SD_{muscle} as the local noise estimate, because we could not set the ROIs in the background air [21, 22].

Apparent diffusion coefficient (ADC) and intravoxel incoherent motion (IVIM)-derived parameters

We analysed the ADC and IVIM-derived parameters from DWI at b-values of 0, 300 and 750 s/mm^2. Under the guidance of an experienced radiologist, one of the researchers set the ROI manually in the submandibular glands, sublingual glands and palatine tonsils using SYNAPSE VINCENT (Fujifilm Medical, Tokyo, Japan), while ensuring that the ROIs were as large as possible and avoiding vessels or gland ducts. The ADCs were calculated from the signal decay curve and approximated by the least squares method. The IVIM theory is shown in the following equation:

$$S_b \big/ S_0 = (1-f) \exp(-b\,D) + f \exp[-b(D + D^*)] \tag{4}$$

Here, S_b and S_0 are signal intensities at arbitrary b value and b = 0 s/mm^2. The IVIM-derived parameters were calculated using a segmented method (Fig. 2) [8]. As the very first step of this method, D was calculated, because the effect of D* on the signal of DWI at b-value higher than 200 s/mm^2 is negligibly small. Therefore, Eq. (4) can be simplified as: Eq. (5).

$$S_{b1}/S_{b2} = \exp[(b_2 - b_1)\,D] \tag{5}$$

Here, S_{b1} and S_{b2} are signal intensities at two b-values higher than 200 s/mm^2.

The second step of the segmented method calculated f as per the following equation:

$$f = (S_0 - S_{inter})/S_0 \tag{6}$$

Here, S_{inter} is the intersection point of the y-axis and the line through ln S_{300} and ln S_{750}. The measurement reproducibility of f and D* were poor; however, inter-slice consistency of f was better than that of D* [23]. Therefore, we evaluated f as the perfusion-related parameter and excluded D* from the analysis.

Statistical analysis

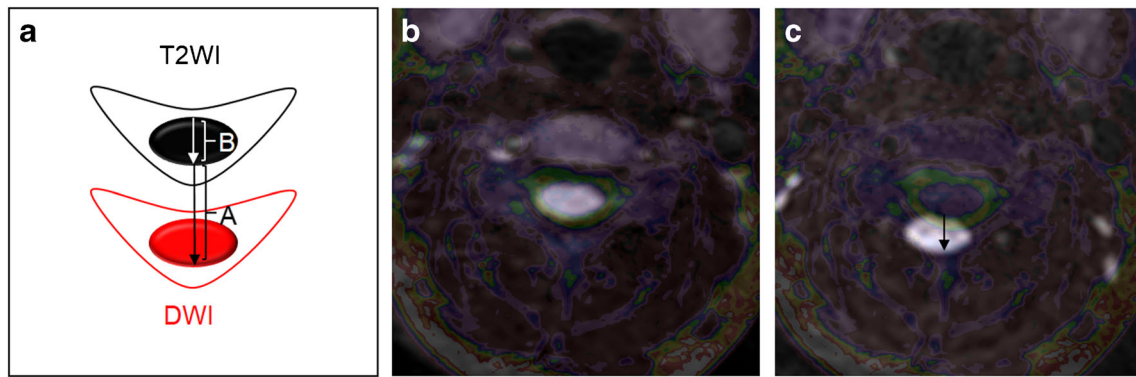Statistical analysis was performed to compare the DR, SNR, CNR, ADC and IVIM-derived parameters of TSE-

Fig. 1 Comparison between image distortion in TSE-DWI and EPI-DWI. (**a**) The schema of fusion images. The black schema represents the spinal cord at T2WI and the red schema represents the distorted spinal cord at DWI. The white arrow shows the maximum diameter of the anatomical structure on T2WI and the black arrow shows the maximum displacement of the anatomical structure between T2WI and each-DWI.

(**b**) The fusion image of TSE- DWI and T2WI. (**c**) The fusion image of EPI-DWI and T2WI. Note that the spinal cord at EPI-DWI (black arrow) (**c**) is more distorted than that at TSE-DWI (**b**). *TSE* turbo spin-echo, *DWI* diffusion-weighted imaging, *EPI* echo-planar imaging, *T2WI* TSE-T2-weighted imaging

DWI and EPI-DWI of each anatomical structure using the Wilcoxon signed-rank test. The statistical significance was set at a p-value less than 0.05. In addition, the reproducibility of the mean ADC and IVIM-derived parameters of TSE-DWI and EPI-DWI were analysed by using the Bland-Altman plot [24], and 95% limits of agreement (LoA) were calculated as a percentage of the overall mean value of the two sequences. The 95% LoA, estimated by mean difference ± 1.96 standard deviation, provides an interval within which 95% of differences between the two methods of measurement are expected to lie [25]. All statistical analyses were performed with JMP Pro 11.0.0 (SAS Institute, Cary, NC, USA).

Fig. 2 Calculation of intravoxel incoherent motion (IVIM)-derived parameters. D is calculated by the equation: $D = - \ln (S_{750}/S_{300})/(750 - 300)$ and f is calculated by the equation: $f = (S_0 - S_{inter})/S_0$. S_{inter} is the intersection point of the Y-axis and the line through $\ln S_{300}$ and $\ln S_{750}$

Results

Comparison of distortion ratio (DR)

The representative two fusion images, which consisted of TSE-DWI with T2WI and EPI-DWI with T2WI, are shown in Figs. 1b and c, respectively. The mean DRs of TSE-DWI and EPI-DWI are shown in Table 1. The distortion in TSE-DWI was significantly smaller than that in EPI-DWI in the cervical spinal cord of the nasopharynx and oropharynx levels, submandibular glands, palatine tonsils and cerebellar hemispheres ($p < 0.05$).

Comparison of signal-to-noise (SNR) and contrast-to-noise (CNR) ratios

The ROI sizes (mean pixels ± SD) at the superior deep cervical lymph node were 85.2 ± 23.5 about TSE-DWI, and 76.4 ± 35.3 about EPI-DWI. The representative images of TSE-DWI and EPI-DWI in a healthy volunteer are shown in Fig. 3. The mean SNRs and CNRs of TSE-DWI and EPI-DWI are shown in Table 2. The SNRs of TSE-DWI were significantly higher than those of EPI-DWI ($p < 0.05$) in the submandibular glands, parotid glands and superior deep cervical lymph node. The CNRs of TSE-DWI were significantly higher than those of EPI-DWI in the submandibular glands and parotid glands ($p < 0.05$). There were no significant differences between the CNRs of TSE-DWI and EPI-DWI in the superior deep cervical lymph node.
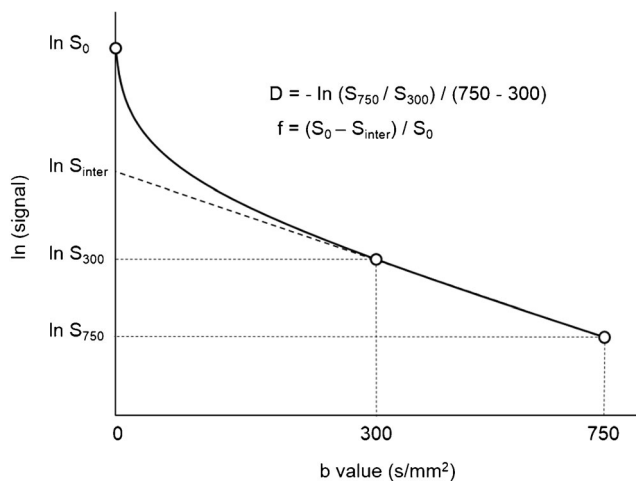
Comparison of ADC and IVIM-derived parameters

The ROI sizes (mean pixels ± SD) at right submandibular gland, left submandibular gland, right sublingual gland, left

Table 1 The DR on TSE-DWI and EPI-DWI

	TSE-DWI	EPI-DWI	p *
Spinal cord (nasopharynx level)	0.35 ± 0.6	1.00 ± 0.8	0.0006
Spinal cord (oropharynx level)	0.13 ± 0.2	0.39 ± 0.2	0.0001
Right submandibular gland	0.10 ± 0.09	0.42 ± 0.3	0.0001
Left submandibular gland	0.11 ± 0.08	0.34 ± 0.2	0.0004
Right palatine tonsil	0.12 ± 0.1	0.58 ± 0.4	0.0001
Left palatine tonsil	0.12 ± 0.1	0.59 ± 0.4	0.0001
Right cerebellar hemisphere	0.035 ± 0.02	0.29 ± 0.1	0.0001
Left cerebellar hemisphere	0.029 ± 0.02	0.26 ± 0.1	0.0001

Data are means ± standard deviations

* Wilcoxon signed rank test

DR distortion ratio, *TSE* turbo spin-echo, *DWI* diffusion-weighted imaging, *EPI* echo-planar imaging

sublingual gland, right palatine tonsil and left palatine tonsil were 432 ± 129, 414 ± 89, 237 ± 67, 224 ± 94, 254 ± 86 and 228 ± 70, respectively, for TSE-DWI, and 438 ± 147, 434 ± 124, 190 ± 58, 172 ± 69, 223 ± 69 and 223 ± 51, respectively, for EPI-DWI. The sublingual glands of two volunteers were excluded, because these could not be depicted in the EPI-DWI. The mean ADC and IVIM-derived parameters of TSE-DWI and EPI-DWI are shown in Table 3. The ADC and D of TSE-DWI exhibited higher values than those of EPI-DWI in the submandibular glands, sublingual glands and palatine tonsils. However, the differences were not significant. The f-value of TSE-DWI was higher than that of EPI-DWI in all parts except the right palatine tonsil. However, the differences were not significant.

Bland-Altman plots are shown in Figs. 4 (a–f); 95% LoA for ADC and IVIM-derived parameters between TSE-DWI and EPI-DWI are shown in Table 4. Fixed biases were not detected; however, Bland-Altman analysis showed wide limits of agreement between TSE-DWI and EPI-DWI (Table 4).

Discussion

Our study results showed that TSE-DWI had significantly smaller image distortion, and higher SNR and CNR in the head and neck than those of EPI-DWI. In general, the TSE sequence, which obtains echo by refocusing RF pulses, is less sensitive to susceptibility artefacts compared to EPI sequence [11]. Reduced image distortion may provide better reproducibility and reliability of diffusion-weighted images and quantitative parameters [10]. Regarding the advantages of TSE-DWI in SNR and CNR, rectangular-shaped and shorter RF pulses might contribute to the improvement of these factors. The image noise depends on the voxel size, receiver bandwidth and number of averages at the image acquisition [26]. In our study, two DWI sequences showed approximately the same voxel size and number of averages; however, the bandwidth of EPI-DWI (2,820 Hz/pixel) was wider than that of TSE-DWI (630 Hz/pixel); therefore, it could significantly affect the SNR and CNR. Sakamoto et al. reported that TSE-DWI has an inherently lower SNR than EPI-DWI [27]. However, our study results conversely revealed that CNR was higher than SNR at submandibular glands and superior deep cervical lymph nodes in TSE-DWI because of setting parameters to maintain image quality suitable for diagnosis. We speculate that the reason why the CNR was much higher than the SNR was that the standard deviation of the signal intensity in the muscle became smaller based on the low signal intensity in DWI at a high b-value.

In the quantitative analyses of ADC and IVIM-derived parameters, no significant difference between TSE-DWI and EPI-DWI was noted; however, TSE-DWI showed higher values than EPI-DWI. There should be many factors accounting for the differences in quantitative parameters between TSE-DWI and EPI-DWI. In the Bland-Altman plot (Fig. 4), the difference in each parameter between TSE-DWI and EPI-DWI might vary depending on volunteers. Additionally, fixed bias or proportional error was not detected in the Bland-Altman plot. Therefore, we speculate that distortion in EPI-
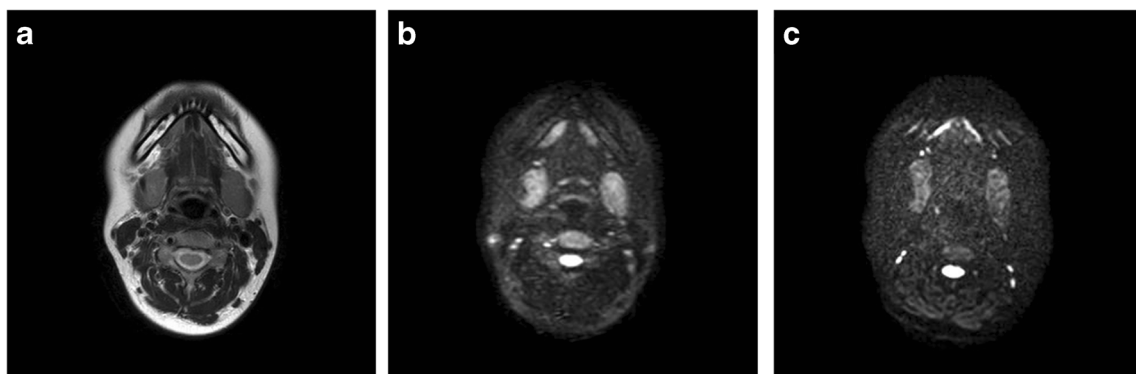

Fig. 3 The axial MR images at the same submandibular gland section of a 22-year-old female volunteer: (**a**) T2WI, (**b**) TSE-DWI of b = 750 and (**c**) EPI-DWI of b = 750. *TSE* turbo spin-echo, *DWI* diffusion-weighted imaging, *EPI* echo-planar imaging, *T2WI* TSE-T2-weighted imaging

Table 2 The SNR and CNR on TSE-DWI and EPI-DWI

	SNR			CNR		
	TSE-DWI	EPI-DWI	p *	TSE-DWI	EPI-DWI	p *
Right submandibular gland	19.8 ± 3.3	10.5 ± 2.1	0.0001	22.3 ± 5.7	9.35 ± 4.7	0.0001
Left submandibular gland	17.9 ± 3.4	9.78 ± 1.5	0.0001	21.1 ± 6.3	9.02 ± 5.7	0.0001
Right parotid gland	18.9 ± 2.8	9.40 ± 2.1	0.0001	13.4 ± 4.2	3.15 ± 2.1	0.0001
Left parotid gland	19.5 ± 3.2	9.88 ± 1.5	0.0001	11.8 ± 5.6	2.44 ± 2.0	0.0001
Superior deep cervical lymph node	7.65 ± 2.1	4.83 ± 1.2	0.0006	39.8 ± 15	29.4 ± 12	0.058

Data are means ± standard deviations

* Wilcoxon signed rank test

SNR signal-to-noise ratio, *CNR* contrast-to-noise ratio, *TSE* turbo spin-echo, *DWI* diffusion-weighted imaging, *EPI* echo-planar imaging

DWI might hamper accurate measurement of quantitative parameters. Image noise can considerably influence the calculation of diffusion parameters [28]. When image noise is large, the diffusion parameters tend to show lower values [28]. TSE-DWI showed higher SNR than EPI-DWI; therefore, the influence of noise was smaller in TSE-DWI. Andreou et al. have reported that the limits of agreement for ADC, D and f in normal liver were −4% to 7%, −5% to 8%, and −24% to 25%, respectively [29]. On the other hand, the limits of agreement for ADC, D and f in our study became much wider (Table 4). Although these results were derived from different ROIs, it would be necessary to show similar LoAs for the follow-up studies. Therefore, there were unacceptable LoAs between TSE-DWI and EPI-DWI in our study. Inaccurate measurement of parameters due to the image distortion on EPI-DWI might be the cause of the wide LoA, although no significant difference between the two DWI sequences was noted. There was a severe distortion in EPI-DWI compared with TSE-DWI, therefore we could not sample the signal intensity from the same region within the organ between low and high b values in EPI-DWI. We speculate that it might affect the calculation of ADC and IVIM-derived parameters

using multiple b values and lead to a wide LoA. Thus, the ADC and IVIM-derived parameters obtained from these two sequences should not be used as equivalent quantitative parameters in disease differentiation, treatment response prediction and prognosis.

There are two major limitations to this study. First, we used the segmented method, which is a non-fitting approach, to measure IVIM-derived parameters for shortening the imaging time by reducing number of b values. Therefore, f-value derived from this method are susceptible to S_0 [30]. Furthermore, the f-value may lack robustness, because it did not take into account the perfusion effect based mainly on higher b values [31]. In addition, the IVIM-derived parameters become more accurate by using a large numbers of b-values. In our study, using only three b-values might have influenced the calculation of IVIM-derived parameters. Second, the acquisition time using three b-values of TSE-DWI (8 min 24 s) was longer than that of EPI-DWI (1 min 42 s). It was impossible to set the same imaging time between TSE-DWI and EPI-DWI in clinical practice, because TSE-DWI has a much longer imaging time than EPI-DWI. We certainly thought that it was ideal to make the same

Table 3 The ADC, D and f on TSE-DWI and EPI-DWI

	ADC			D			f		
	TSE-DWI	EPI-DWI	p *	TSE-DWI	EPI-DWI	p *	TSE-DWI	EPI-DWI	p *
Right submandibular gland	1.19 ± 0.08	1.15 ± 0.13	0.23	0.93 ± 0.13	0.92 ± 0.15	0.86	18.9 ± 8.01	16.8 ± 5.32	0.54
Left submandibular gland	1.23 ± 0.07	1.13 ± 0.12	0.094	0.95 ± 0.08	0.86 ± 0.19	0.08	20.0 ± 5.95	19.5 ± 9.48	0.95
Right sublingual gland	1.24 ± 0.13	1.23 ± 0.18	0.62	1.00 ± 0.16	1.00 ± 0.19	0.97	17.1 ± 8.20	16.3 ± 11.1	0.97
Left sublingual gland	1.21 ± 0.13	1.15 ± 0.14	0.15	0.93 ± 0.12	0.91 ± 0.18	0.73	20.0 ± 8.03	17.2 ± 8.35	0.73
Right palatine tonsil	0.88 ± 0.09	0.83 ± 0.12	0.24	0.70 ± 0.09	0.63 ± 0.11	0.068	13.0 ± 6.41	15.2 ± 6.64	0.3
Left palatine tonsil	0.88 ± 0.10	0.82 ± 0.13	0.091	0.70 ± 0.12	0.68 ± 0.12	0.67	13.2 ± 4.97	10.4 ± 5.04	0.17

Data are means ± standard deviations

Units of ADC and D are 10^{-3} mm^2/s, and that of f is %. * Wilcoxon signed rank test *ADC* apparent diffusion coefficients, *TSE* turbo spin echo, *DWI* diffusion-weighted imaging, *EPI* echo planar imaging, *D* pure diffusion coefficients, *f* perfusion fraction
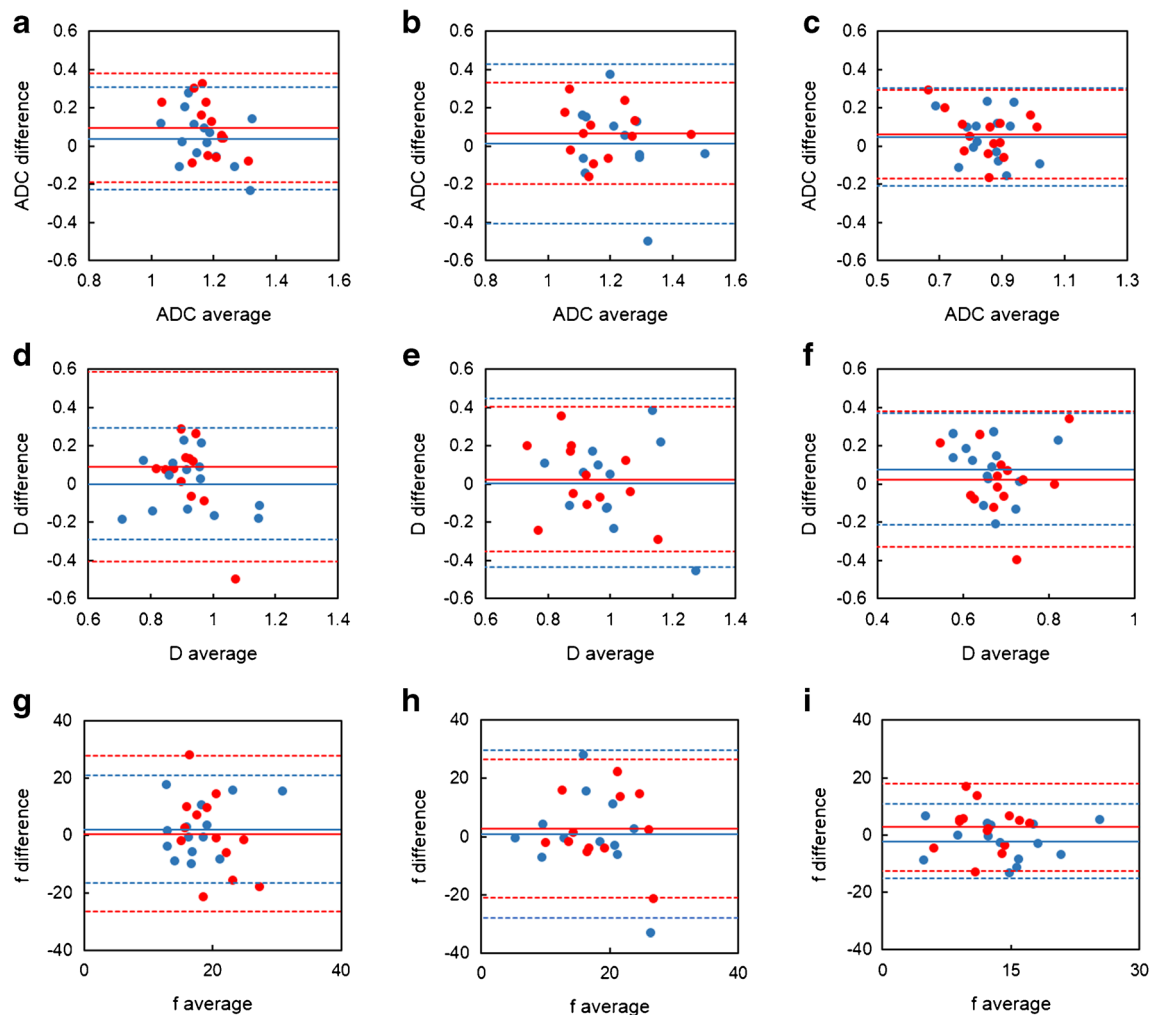
Fig. 4 Bland-Altman plots for ADC, D and f of TSE-DWI and EPI-DWI in the bilateral submandibular glands (**a**, **d**, **g**), sublingual glands (**b**, **e**, **h**) and palatine tonsils (**c**, **f**, **i**). Each colour (blue = right anatomical regions, red = left anatomical regions) plot shows the value difference against the value average between TSE-DWI and EPI-DWI. Continuous lines show average measurement difference and dotted lines show 95% limits of agreement. *TSE* turbo spin-echo, *DWI* diffusion-weighted imaging, *EPI* echo-planar imaging, *T2WI* TSE-T2-weighted imaging

Table 4 The LoA for ADC and IVIM parameters between TSE-DWI and EPI-DWI

| | LoA (%) | | |
	ADC	D	f
Right submandibular gland	−19.2, 26.4	−32.2, 32.8	−100.3, 120.2
Left submandibular gland	−16.5, 33.3	−44.8, 68.4	−135.5, 153.4
Right sublingual gland	−32.3, 34.9	−38.7, 40.5	−144.0, 163.2
Left sublingual gland	−18.0, 29.4	−39.3, 46.8	−104.2, 135.6
Right palatine tonsil	−24.6, 36.3	−32.1, 56.5	−157.9, 125.8
Left palatine tonsil	−22.6, 38.8	−47.0, 54.2	−125.3, 173.3

LoA limits of agreement, *ADC* apparent diffusion coefficients, *IVIM* intravoxel incoherent motion, *TSE* turbo spin echo, *DWI* diffusion-weighted imaging, *EPI* echo planar imaging, *D* pure diffusion coefficients, *f* perfusion fraction

imaging time and parameters as identical as possible between the two sequences, but we set those as clinically applicable sequences subject to limited imaging time. These discrepancies including a small number of b-factors will have affected the measurement of the DR, SNR, CNR, ADC and IVIM-derived parameters. The longer the acquisition time, the greater the sensitivity to motion artefacts; this consequently influences the quantitative parameters. However, these artefacts were not visually observed in our study. In clinical practice, it is necessary to reduce the acquisition time to adopt TSE-DWI for assessment of diseased patients. A comparative study of image quality or IVIM-derived parameters calculated by the fitting approach using large numbers of b-values between TSE-DWI acquired in a shorter imaging time and EPI-DWI including readout-segmented multi-shot sequence that could reduce artefacts is needed in a future.

In conclusion, TSE-DWI can improve image quality in comparison with EPI-DWI in head and neck imaging. Therefore, TSE-DWI could be a good alternative to EPI-DWI for patients sensitive to distortion such as those with metallic implants. However, it could not be recommended using both TSE-DWI and EPI-DWI in follow-up studies in the same patients, because TSE-DWI might show higher ADC, D and f values compared with EPI-DWI.

References

1. Schaefer PW, Grant PE, Gonzalez RG (2000) Diffusion-weighted MR imaging of the brain. Radiology 217:331–345
2. Tien RD, Felsberg GJ, Friedman H, Brown M, MacFall J (1994) MR imaging of high-grade cerebral gliomas: value of diffusion weighted echo planar pulse sequences. AJR 162:671–677
3. Okamoto K, Ito J, Ishikawa K, Sakai K, Tokiguchi S (2000) Diffusion-weighted echo-planar MR imaging in differentiation diagnosis of brain tumors and tumor-like conditions. Eur Radiol 10: 1342–1350
4. Tsuchiya K, Katase S, Yoshino A, Hachiya J (1999) Diffusion-weighted MR imaging of encephalitis. AJR 173:1097–1099
5. Kim S, Loevner L, Quon H et al (2009) Diffusion-weighted magnetic resonance imaging for predicting and detecting early response to chemoradiation therapy of squamous cell carcinomas of the head and neck. Clin Cancer Res 15:986–994
6. Wang J, Takashima S, Takayama F et al (2001) Head and neck lesions: characterization with diffusion-weighted echo-planar MR imaging. Radiology 220:621–630
7. Le Bihan D, Breton E, Lallemand D, Aubin ML, Vignaud J, Lavel-Jeantet M (1988) Separation of diffusion and perfusion in intravoxel incoherent motion MR imaging. Radiology 168:497–505
8. Sumi M, Van Cauteren M, Sumi T, Obara M, Ichikawa Y, Nakamura T (2012) Salivary gland tumors: use of intravoxel incoherent motion MR imaging for assessment of diffusion and perfusion for the differentiation of benign from malignant tumors. Radiology 263:770–777
9. Hauser T, Essig M, Jensen A et al (2013) Characterization and therapy monitoring of head and neck carcinomas using diffusion-imaging-based intravoxel incoherent motion parameters – preliminary results. Neuroradiology 55:527–536
10. Verhappen MH, Pouwels PJ, Ljumanovic R et al (2012) Diffusion-weighted MR imaging in head and neck cancer: comparison between half-fourier acquisition single-shot turbo spin-echo and EPI techniques. AJNR 33:1239–1246
11. Sigmund EE, Jensen J (2011) Basic physical principles of body diffusion-weighted MRI. In: Taouli B (ed) Extra-cranial Applications of Diffusion-weighted MRI. Cambridge University Press, Cambridge, pp 1–17
12. Yoshino N, Yamada I, Ohbayashi N et al (2001) Salivary glands and lesions: evaluation of apparent diffusion coefficients with split-echo diffusion-weighted MR imaging initial report. Radiology 221:837–842
13. Thoeny HC, De Keyzer F, King AD et al (2012) Diffusion-weighted MR imaging in the head and neck. Radiology 263:19–32
14. De Foer B, Vercruysse JP, Pilet B et al (2006) Single-shot, turbo spin-echo, diffusion-weighted imaging in the detection of acquired middle ear cholesteatoma. AJNR 27:1480–1482
15. Yoshida T, Urikura A, Shirata K, Nakaya Y, Terashima S, Hosokawa Y et al (2016) Image quality assessment of single-shot turbo spin echo diffusion-weighted imaging with parallel imaging technique: a phantom study. Br J Radiol 89:20160512
16. Elefante A, Cavaliere M, Russo C et al (2015) Diffusion weighted MR imaging of primary and recurrent middle ear cholesteatoma: an assessment by readers with different expertise. Biomed Res Int: 1–7
17. Kolff-Gart AS, Pouwels PJW, Noij DP (2015) Diffusion-weighted imaging of the head and neck in healthy subjects: reproducibility of ADC values in different MRI system repeat session. AJNR Am J Neuroradiol 36:384–390
18. Kamimura K, Nakajo M, Fukukura Y, et al (2016) Intravoxel incoherent motion in normal pituitary gland: initial study with turbo spin-echo diffusion-weighted imaging. AJNR Am J Neuroradiol 1–6
19. Fujima N, Yoshida D, Sakashita T et al (2014) Intravoxel incoherent motion diffusion-weighted imaging in head and neck squamous carcinoma: assessment of perfusion-related parameters compared to dynamic contrast-enhanced MRI. Magn Reson Imaging 32:1206–1213
20. Koyasu S, Lima M, Umeoka S et al (2014) The clinical utility of reduced-distortion readout-segmented echo-planar imaging in the head and neck region: initial experience. Eur Radiol 24:3088–3096
21. Moon WJ (2007) Measurement of signal-to-noise ratio in MR imaging with sensitivity encoding. Radiology 243:908–909
22. Heverhagen JT (2007) Noise measurement and estimation in MR imaging experiments. Radiology 245:638–639
23. Marzi S, Piludu F, Vidiri A (2013) Assessment of diffusion parameters by intravoxel incoherent motion MRI in head and neck squamous cell carcinoma. NMR Biomed 26:1806–1814
24. Bland JM, Altman DG (1986) Statistical methods for assessing agreement between two methods of clinical measurement. The Lancent 327:307–310
25. Bland JM, Altman DG (1999) Measuring agreement in method comparison studies. Stat Methods Med Res 8:135–160
26. Edelstein WA, Glover GH, Hardy CJ, Rendington RW (1986) The intrinsic signal-to-noise ratio in NMR imaging. Magn Reson Med 3:604–618
27. Sakamoto J, Sasaki Y, Otonari-Yamamoto M, Nishikawa K, Sano T (2012) Diffusion-weighted imaging of the head and neck with HASTE: influence of imaging parameters on image quality. Oral Radiol 28:87–94

28. Dietrich O, Heiland S, Sartor K (2001) Noise correction for the exact determination of apparent diffusion coefficients at low SNR. Magn Reson Med 45:448–453

29. Andreou A, Koh DM, Collins DJ et al (2013) Measurement reproducibility of perfusion fraction and pseudodiffusion coefficient derived by intravoxel incoherent motion diffusion-weighted MR imaging in normal liver and metastases. Eur Radiol 23:428–434

30. Suo S, Lin N, Wang H et al (2015) Intravoxel incoherent motion diffusion-weighted MR imaging of breast cancer at 3.0 tesla: Comparison of diffusion curve-fitting methods. J Magn Reson Imaging 42:362–370

31. Le Bihan D (2008) Intravoxel incoherent motion perfusion MR inaging: a wake-up call. Radiology 249:748–752